Instability of modified Zakharov-Kuznetsov solitons in an inhomogeneous partially degenerate electron-ion magnetoplasma

M. Irfan *

Department of Physics, University of Malakand Chakdara Dir(L), Khyber Pakhtun Khwa 18800, Pakistan

(Received 30 March 2022; revised 19 August 2022; accepted 2 December 2022; published 20 December 2022)

Linear and nonlinear propagation characteristics of multidimensional drift ion-acoustic (IA) solitons are studied in an inhomogeneous partially degenerate electron-ion magnetoplasma. A modified Zakharov-Kuznetsov (mZK) equation is deduced, accounting for the longitudinal as well as the transverse dispersions. It is shown that the mZK equation admits a distinct solution, revealing excitation of a pulse-shaped soliton when the phase speed exceeds by the wave dispersion. For the instability condition of the waves, a novel growth rate (γ) is derived by modifying the standard small-k expansion scheme. The instability criterion, given for long-wavelength IA waves, has not been described elsewhere. Numerical analysis show that solitary pulses gain energy from the ion drift, involving into instability: it saturates with amplification of the unstable potentials. Similarly trapped electrons lead to unstable growth of the solitary waves by enhancing γ. This study is relevant to compact stars and to high-density facilities where density inhomogeneity ensues the unstable drift modes. The instability analysis is important in understanding anomalous diffusion, which reduces the lifespan ($\tau = \gamma^{-1}$) of magnetically confined plasma.

DOI: 10.1103/PhysRevE.106.065204

I. INTRODUCTION

A warm ionized matter, containing degenerate constituents, constitutes partially degenerate plasma. The latter has gained considerable importance in the investigation of coherent modes and instabilities in high-density plasmas, modified by modest thermal correction. The nanoscale objects such as tunneling diodes [1], quantum dots [2], quantum wells [3], nanotubes [4], etc., are technologically important scenarios for the partially degenerate ionized matter. Such plasmas have also stabilized the compact stars [5,6], e.g., white dwarfs, magnetars, and neutron stars, against their self-gravitational collapse. Similarly, a degenerate plasma with nonvanishing thermal effect emerges when matter is irradiated by intensified laser [7,8]. The quantum corrections of the plasma state, namely, degeneracy pressure, quantum diffusion, spin correlation, etc., therein [7,8] arise when thermal de Broglie wavelength $\lambda_{\rm j}(=\hbar/m_{\rm j}{\rm v_j})$ of the lighter plasma species approaches or exceeds the Wigner-Seitz radius $a(=\sqrt[3]{3/4\pi N_0})$. Here $\hbar(=h/2\pi)$ is the reduced Planck constant, N_0 the equilibrium number density, and $m_{\rm j}({\rm v_j})$ stands for the mass (speed) of the jth degenerate particulate. The aspects of degenerate particles noticeably alter with variations in state variables (e.g., number density, temperature, and magnetic field) of a dense plasma.

Bernstein *et al.* [9] first proposed the concept that an electric potential adiabatically traps a charged particle whose potential energy is greater than its kinetic energy. Gurevich *et al.* [10] had extended the theory to an electron-ion (EI) plasma by verifying that solitary excitations adiabatically trap electrons. Later, many researchers elaborated the impact of trapped particles on the wave dynamics. In this context it was noted that trapped particles evolve unstable modes that modify the confinement parameters [11] in fusion plasma. Similarly, drift waves due to trapped electrons [12] amplify random perturbations and hence deconfine magnetoplasma. In contrast, particles trapped in a magnetic mirror [13] overcome loss of matter. The impact of trapped particles on wave dynamics has also been confirmed in manifold observations. For instance, the broadband noise in the magnetosphere [14] has been recognized as the electrostatic perturbations, excited by trapped electrons. It has been confirmed that the excitation of the wake field in lithium-helium plasmas [15] trap electrons, which in turn emit amplified optical pulses. Apart from the trapped constituents, finite (but nonzero) thermodynamic temperature also gives rise to untrapped particulate, constituting partially degenerate plasmas. Thus Shah *et al.* [16] have noticed that trapped and untrapped electrons in partially degenerate EI plasma significantly modify the amplitude and the spatial extension of ion-acoustic (IA) solitons. Tsintsadze *et al.* [17] have reported that trapped electrons favor excitation of the solitary potentials by extending the domain of Mach numbers. Recently, Irfan *et al.* [18] have shown that trapped electrons evolve modulational instability by piling up the harmonic waves.

Low-frequency drift modes were extensively evaluated for bulk heating of charged species and anomalous diffusion in plasmas. It was confirmed [11] that propagation of drift waves in magnetoplasma is accompanied by excitations of vortices that cause diffusion of charges. These waves effectively conduct heat into the fusion plasma [11] when the confinement period saturates. Similarly, the scattering of ions due to drift potentials [19] evolve the plasma

*mirfankhan1982@gmail.com

turbulence. Vianello *et al.* [20] have shown that nonlinear drift waves ensue the Alfv*é*nic turbulence and in turn heat magnetoplasma. Salimullah *et al.* [21] have pointed out that streaming effect in dusty plasma causes instability of the drift acoustic perturbations. Note that unstable waves can be observed in timescales of the order of the propagation period or less, because these excitations experience a temporal growth of the perturbations. For stability analysis of multidimensional coherent excitations, various algebraic techniques were introduced. By employing a series expansion method, Montgomery [22] had deduced a Bernstein-Greene-Kruskal equilibrium that describes the stability condition of the arbitrary amplitude waves. Later, Rowlands [23] derived a stability criterion for counterstreaming waves by modifying the series expansion scheme. Infeld [24]—introducing a standard small-k expansion technique—deduced the growth rate of cnoidal waves. Similarly, Mamun and Cairns [25] described the stability analysis for Zakharov-Kuznetsov solitons that are superimposed by plane perturbations. They noticed that the obliquity parameter (magnetic field) reduces (enhances) the growth rate of the solitary pulses. This study elucidates the evolution and the stability analysis of modified Zakharov-Kuznetsov (mZK) solitons propagating in an inhomogeneous partially degenerate EI magnetoplasma. Thus, by modifying the small-k expansion scheme, the growth rate of the mZK solitons is obtained that is not elaborated elsewhere [24,25].

The layout of this manuscript is as follows: Section II presents the dimensionless quantum magnetohydrodynamic (QMHD) equations that describe multidimensional propagation of the drift ion-acoustic waves in an inhomogeneous partially degenerate EI magnetoplasma. Thus by solving the QMHD equations, an mZK equation is deduced that admits a distinct solution for the IA solitary potentials as elaborated in Sec. III. In Sec. IV an instability growth rate for the mZK solitons is derived by modifying the small-k expansion method. The important results, pertinent to the novel growth rate, are discussed in Sec. V, while the conclusion is briefly summarized in Sec. VI.

II. GOVERNING EQUATIONS AND MODEL

To examine the propagation characteristics and the stability (instability) of modified drift IA solitons, an inhomogeneous partially degenerate EI magnetoplasma is chosen. Owing to finite (but nonzero) plasma temperature, the electron fluid is taken as partially degenerate Fermi gas containing the trapped and the untrapped constituents. The plasma is embedded in a uniform external magnetic field $\mathbf{B}(=B_0\hat{Z})$, acting in the Z direction. Here B_0 is the magnitude of magnetic field, whereas $\hat{Z}$ stands for direction of the z axis. The density gradient of plasma is given by $\nabla N_0\{=-\hat{\mathbf{X}}\partial N_0(X)/\partial X\}$ and corresponds to inhomogeneity along the x axis, where $N_0(X)$ and ∇ designate the equilibrium density function and spatial operator, respectively. The quasineutrality condition at equilibrium demands choice of $N_{i0}(X)\ \approx N_{e0}(X)\ \equiv N_0(X)$, where $N_{i0}(X)$ and $N_{e0}(X)$ represent the equilibrium density functions for the ions and the electrons, respectively. Thus the evolution of multidimensional drift IA excitations is governed by the following QMHD [18] equations:

$$\frac{\partial \bar{N}}{\partial \bar{T}}+\bar{\nabla}\cdot(\bar{N}\bar{\mathbf{U}})=0, \tag{1}$$

$$\frac{\partial \bar{\mathbf{U}}}{\partial \bar{T}}+(\bar{\mathbf{U}}\cdot\bar{\nabla})\bar{\mathbf{U}}+\bar{\nabla}\bar{\Phi}-\bar{\omega}_r(\bar{\mathbf{U}}\times\hat{\mathbf{Z}})=0, \tag{2}$$

and

$$\bar{\nabla}^2\bar{\Phi}-(\bar{N}_e-\bar{N})=0. \tag{3}$$

Here the dimensionless variables $\bar{\mathbf{U}}(=U/C_s)$ and $\bar{N}(=N/N_0)$ are the velocity and the number density of ions, respectively, $\bar{\Phi}(=e\phi/\mathcal{E}_{\rm Fe})$ the electric potential; moreover, $\bar{T}(=\omega_{pi}T)$ is the temporal variable and $\bar{\nabla}(=\lambda_{\rm Fe}\nabla)$ stands for the spatial operator. The plasma frequency, Fermi length, and Fermi acoustic speed are respectively given as $\omega_{pi}(=\sqrt{4\pi e^2N_0/m_i})$, $\lambda_{\rm Fe}(=\sqrt{\mathcal{E}_{\rm Fe}/4\pi e^2N_0})$, and $C_s(=\sqrt{\mathcal{E}_{\rm Fe}/m_i})$ with electron Fermi energy $\mathcal{E}_{\rm Fe}\{=\hbar^2(3\pi^2N_0)^{2/3}/2m_e\}$. The gyro-to-plasma frequency ratio is given as $\bar{\omega}_r(=\omega_{ci}/\omega_{pi})$, where $\omega_{ci}(=eB_0/m_ic)$ is the ion gyrofrequency, $e(m_i)$ denotes the electric charge of electron (mass of ion), and c corresponds to the vacuum speed of light. Note that the QMHD equations (1)–(3) describe evolution of the nonlinear electrostatic excitations [26] whose wavelength is much larger as compared to the Fermi length (i.e., $\lambda\gg\lambda_{\rm Fe}$). Thus the QMHD model cannot account for the kinetic effects, e.g., Landau damping, multiplasmon resonances, spin-orbit interactions, etc., arising at much shorter length scales. More importantly, these equations remain valid as long as the kinetic energy of degenerate constituents is greater than their interaction energy. As the simplified QMHD model has not incorporated the spin (relativistic) correction, therefore it holds when spin energy (phase speed) of degenerate particles (a wave) is much smaller as compared to the Fermi energy (vacuum speed of light). The dimensionless electron density function $\bar{N}_e(=N_e/N_0)$ for a partially degenerate EI magnetoplasma [16,18] is given by

$$\bar{N}_e=\bar{N}_0(X)\{(1+\bar{\Phi})^{\frac{3}{2}}+\Theta^2(1+\bar{\Phi})^{\frac{-1}{2}}\}, \tag{4}$$

where $\Theta(=\pi\mathcal{T}_e/\sqrt{8}\mathcal{E}_{\rm Fe})$ is the temperature ratio, $\mathcal{T}_e$ the electron temperature, and $\bar{N}_0(X)\{=N_0(X)/N_0\}$ corresponds to the dimensionless equilibrium electron density. See from Eq. (4) that finite temperature $(\Theta>0)$ deviates the plasma from perfect degeneracy [27], giving rise to trapped electrons as well as untrapped electrons. It has been shown [9] that an electron, attaining negative or zero net energy (i.e., $\mathcal{E}\leqslant 0$) in a wave potential, is adiabatically trapped. Contrary to this, the electron has unrestricted dynamics at $\mathcal{E}>0$, known as the untrapped electron. Thus the first (second) parenthetical term on the right-hand side in Eq. (4), evaluated at $\mathcal{E}\leqslant(>)0$, represents the trapped (untrapped) electrons, as illustrated in Refs. [28,29]. The compact stars contain warmly dense magnetoplasma [27,30], described by the faint luminosity spectra. The electron temperature in neutron stars (white dwarfs) varies up to 10^9 K($\sim 2\times10^7$ K), and the degeneracy parameter turns out to be $X_{\rm Fe}(=\mathcal{E}_{\rm Fe}/\mathcal{T}_e)>1$. Thus the ionized matter in compact objects attains a partially degenerate state, comprised of trapped and untrapped electrons, and is therefore appropriately described by Eq. (4). For a perfect degenerate electron gas when $\Theta\approx 0$, the second parenthetical term in Eq. (4) vanishes: it corresponds to the density function of degenerate trapped electrons. Moreover, by setting $\bar{\Phi}=0$ in Eq. (4), one obtains the equilibrium number density of partially degenerate electrons as $\bar{\mathcal{N}}_0=\bar{N}_0(X)(1+\Theta^2)$. Upon substituting Eq. (4) in Eq. (3), one arrives at

$$(\beta-\bar{\nabla}^2)\bar{\Phi}-\bar{N}\approx 0, \tag{5}$$

where $\beta=\bar{N}_0(X)(3-\Theta^2)/2$ is the inverse-square screening length for partially degenerate EI magnetoplasma. Thus the dimensionless QMHD equations (1), (2), and (5) may describe evolution of the multidimensional IA waves, impacted by the ion drift. The bar (−) over physical variables is dropped from here forward for simplicity.

A. Linear wave analysis

In order to study the propagation characteristics of the linear drift IA wave, a plane wave solution is chosen by substituting $\partial/\partial T=-i\omega$ in Eqs. (1), (2), and (5). Here ω is the angular frequency, and $i(=\sqrt{-1})$ stands for an imaginary number. As the angular frequency of the wave is much smaller as compared to the ion gyrofrequency [11], therefore $\partial/\partial T\ll\omega_r$ condition holds. Thus solving Eqs. (1) and (2), one obtains

$$-i\omega N+\mathcal{N}_0\left(-\mathcal{K}_iU_X+\frac{\partial U_X}{\partial X}+\frac{\partial U_Y}{\partial Y}+\frac{\partial U_Z}{\partial Z}\right)=0, \tag{6}$$

$$U_X\approx-\frac{1}{\omega_r}\frac{\partial\Phi}{\partial Y}, \tag{7}$$

$$U_Y\approx\frac{i\omega}{\omega_r^2}\frac{\partial\Phi}{\partial Y}, \tag{8}$$

and

$$U_Z\approx-\frac{i}{\omega}\frac{\partial\Phi}{\partial Z}. \tag{9}$$

The parameter $\mathcal{K}_i(=-\partial N_0(X)/N_0(X)\partial\bar{X})$ computes inhomogeneity of the dynamical ions in inhomogeneous magnetoplasma. The former simplifies into the equilibrium density function as $N_0(X)=N_0\exp(-\mathcal{K}_iX)$, where N_0 and $N_0(X)$ are the ion number density at $X=0$ and $X>0$, respectively. The potential gradients act in the YZ plane (i.e., $\partial\Phi/\partial Y$ and $\partial\Phi/\partial Z$); therefore I have chosen $\partial\Phi/\partial X=0$ in obtaining Eqs. (6) and (7). The Lorentz force gives rise to ion drift along the x axis, therefore constituting a drift IA wave. The plasma has relevance to toroidal devices [11], where radial variations in the electrostatic potential are vanishingly small. Equations (6) and (7) reduce into the ion number density as

$$N=\frac{\mathcal{N}_0}{\omega^2}\left(\frac{\omega^2}{\omega_r^2}\frac{\partial^2\Phi}{\partial Y^2}-\frac{\partial^2\Phi}{\partial Z^2}-\frac{i\omega\mathcal{K}_i}{\omega_r}\frac{\partial\Phi}{\partial Y}\right). \tag{10}$$

By imposing the plane wave approximation, as $\Phi\sim\exp\{i(k_\perp Y+k_\parallel Z-\omega T)\}$, Eqs. (5) and (10) lead to the following linear dispersion relation of the drift IA wave:

$$\left(\beta+k^2+\mathcal{N}_0\mathrm{v}_\mathrm{E}^2\right)\omega^2-\mathcal{N}_0\omega_*\omega-\mathcal{N}_0{k_\parallel}^2=0. \tag{11}$$

Here $\mathrm{v}_\mathrm{E}(=k_\perp/\omega_r)$ represents the electric drift, $k(=\sqrt{k_\parallel^2+k_\perp^2})$ the wave number, and $k_\parallel(k_\perp)$ is the component of k in the parallel (perpendicular) direction of B_0. Moreover, the drift frequency and the drift speed are given by $\omega_*(=\mathrm{v}_\mathrm{D}k_\perp)$ and $\mathrm{v}_\mathrm{D}(=\mathcal{K}_i/\omega_r)$, respectively. The quadratic equation (11) admits roots ω_+ and ω_-, holding $\omega_+>0$ and $\omega_-<0$ conditions, respectively. Thus ω_+ (ω_-) is the frequency of drift IA wave, propagating in the direction of (opposite to) B_0. See the real values for ω_+ and ω_-(i.e., $\omega_+^2>0$ and $\omega_-^2>0$), revealing that the inhomogeneous, partially degenerate EI magnetoplasma is convectively stable to propagation of linear drift IA excitations. Thus, using Eq. (11), one obtains phase speed $U_p(=\omega/k_\parallel)$ of the drift IA waves, as

$$U_{p\pm}=\frac{\frac{\mathcal{N}_0\mathrm{v}_\mathrm{D}k_\perp}{2k_\parallel}\pm\frac{1}{2}\left\{\left(\frac{\mathcal{N}_0\mathrm{v}_\mathrm{D}k_\perp}{k_\parallel}\right)^2+4\mathcal{N}_0\left(\beta+k^2+\mathcal{N}_0\mathrm{v}_\mathrm{E}^2\right)\right\}^{\frac{1}{2}}}{\beta+k^2+\mathcal{N}_0\mathrm{v}_\mathrm{E}^2}, \tag{12}$$

where $U_{p+}(U_{p-})$ is the phase speed of drift IA wave that propagates in the direction of (opposite to) B_0. Equation (12) illustrates that the phase speed $(U_{p\pm})$ tapers off as the electric potential decreases.

III. MODIFIED ZAKHAROV-KUZNETSOV EQUATION

To examine the evolution of nonlinear mZK solitary waves, one uses the iteration method [31] for simplifying the expression of angular frequency. Thus in the long-wavelength (low-frequency) limit, setting $\nabla^2\ll\beta$ and $\omega\ll\omega_r$ conditions in Eqs. (5) and (10), one obtains $\omega^2\approx-\mathcal{N}_0\partial^2/\beta\partial Z^2$ [11]. The latter, combined with Eq. (10), is substituted in Eq. (5) and simplified to obtain

$$\omega^2(\beta-\nabla^2)\Phi+\mathcal{N}_0\left(\frac{\mathcal{N}_0}{\beta\omega_r^2}\frac{\partial^4\Phi}{\partial Y^2\partial Z^2}+\frac{\partial^2\Phi}{\partial Z^2}-\frac{\mathrm{v}_\mathrm{D}\mathcal{N}_0^{\frac{1}{2}}}{\beta^{\frac{1}{2}}}\frac{\partial^2\Phi}{\partial Y\partial Z}\right)=0. \tag{13}$$

It can be readily checked that Eq. (13) reduces into the result obtained in Ref. [32] when one replaces β by the corresponding factor therein [32]. Substituting $\partial/\partial Y=ik_\perp$ and $\partial/\partial Z=ik_\parallel$ in Eq. (13), one arrives at

$$\omega\approx\frac{\mathcal{N}_0^{\frac{1}{2}}}{\beta^{\frac{1}{2}}}\left\{1-\frac{{k_\perp}^2}{2\beta}\left(1+\frac{\mathcal{N}_0}{\omega_r^2}\right)-\frac{{k_\parallel}^2}{2\beta}\right\}k_\parallel-\frac{\mathrm{v}_\mathrm{D}k_\perp\mathcal{N}_0}{2\beta}\left(1-\frac{{k_\parallel}^2}{2\beta}\right). \tag{14}$$

Solving Eqs. (9) and (14) together, the following expression is deduced:

$$\frac{\partial\Phi}{\partial Z}=\frac{\mathcal{N}_0^{\frac{1}{2}}}{\beta^{\frac{1}{2}}}\left(\frac{\partial U_Z}{\partial Z}-\frac{\mathrm{v}_D\mathcal{N}_0^{\frac{1}{2}}}{2\beta^{\frac{1}{2}}}\frac{\partial U_Z}{\partial Y}+\frac{1+\frac{\mathcal{N}_0}{\omega_r^2}}{2\beta}\frac{\partial^3U_Z}{\partial Y^2\partial Z}+\frac{1}{2\beta}\frac{\partial^3U_Z}{\partial Z^3}-\frac{\mathrm{v}_D\mathcal{N}_0^{\frac{1}{2}}}{4\beta^{\frac{3}{2}}}\frac{\partial^3U_Z}{\partial Y\partial Z^2}\right). \tag{15}$$

Equation (15) is substituted into Eq. (2) that upon simplification leads to the modified Zakharov-Kuznetsov equation, as

$$\frac{\partial U_Z}{\partial T}+U_Z\frac{\partial U_Z}{\partial Z}+\frac{\partial}{\partial Z}\left(\mathrm{A}+\mathrm{B}\frac{\partial^2}{\partial Y^2}+\mathrm{C}\frac{\partial^2}{\partial Z^2}\right)U_Z + \frac{\partial}{\partial Y}\left(\mathrm{D}+\mathrm{E}\frac{\partial^2}{\partial Z^2}\right)U_Z=0. \tag{16}$$

The coefficients A and D (B, C, and E), appearing in Eq. (16), account for the lower (higher) order dispersions of the drift IA wave, given by

$$\mathrm{A}=\left(\frac{\mathcal{N}_0}{\beta}\right)^{\frac{1}{2}},\ \ \mathrm{B}=\frac{\mathrm{A}}{2\beta}\left(1+\frac{\mathcal{N}_0}{\omega_r^2}\right),$$

and

$$\mathrm{C}=\frac{\mathrm{A}}{2\beta},\ \ \mathrm{D}=-\frac{\mathrm{v_D}\mathrm{A}^2}{2},\ \text{ and }\ \mathrm{E}=-\frac{\mathrm{v_D}\mathrm{A}^2}{4\beta^2}.$$

Equation (16) is essentially different from the (p,2p)-mZK equation, illustrated in Ref. [33]. The former describes nonlinear drift IA excitations, suffered by enhanced wave dispersions (accounted by coefficients A to E) in the parallel and perpendicular directions of B_0. Thus, setting $\mathrm{A}=\mathrm{D}=\mathrm{E}=0$ in Eq. (16) while taking $\mathrm{A}=1$, $\mathrm{B}=0$, and $p=1$ in the (p,2p)-mZK equation therein [33], the evolution equations reduce into the ZK equation that leads to excitation of weakly nonlinear and weakly dispersive solitary potentials. More importantly, the mZK equation (16) admits a distinct solitary wave solution; it is not elaborated in the earlier studies [24,25], as given in the forthcoming analysis.

A. Modified Zakharov-Kuznetsov solitons

For stationary solution of the mZk equation (16), the coordinate axes (Y,Z) are rotated by an angle θ that leads to transformation of the independent variables [34–37], as

$$\zeta=Y\cos\theta-Z\sin\theta,\ \ \eta=Y\sin\theta+Z\cos\theta,\ \text{ and }\ \tau=T. \tag{17}$$

Substituting Eq. (17) into Eq. (16), one obtains

$$\frac{\partial\Phi}{\partial\tau}+L_1\Phi\frac{\partial\Phi}{\partial\eta}+L_2\frac{\partial^3\Phi}{\partial\eta^3}+L_3\Phi\frac{\partial\Phi}{\partial\zeta}+L_4\frac{\partial^3\Phi}{\partial\zeta^3} + L_5\frac{\partial^3\Phi}{\partial\eta^2\partial\zeta}+L_6\frac{\partial^3\Phi}{\partial\eta\partial\zeta^2}+L_7\frac{\partial\Phi}{\partial\zeta}+L_8\frac{\partial\Phi}{\partial\eta}=0. \tag{18}$$

Here L_j represents the nonlinearity and the dispersion coefficients, already given in Appendix A. The index j takes positive integral values, as $j=1,2....,8$. For a steady-state wave solution of Eq. (18), a comoving variable is chosen [38] as $\mathcal{Z}=\eta-U_{p+}\tau$. Thus the spatial and temporal operators of the coordinate (ζ,η) transform as $\partial/\partial\eta\rightarrow\partial/\partial\mathcal{Z}$, $\partial/\partial\zeta\rightarrow0$, $\partial^2/\partial\zeta^2\rightarrow0$, $\partial^3/\partial\zeta^3\rightarrow0$, and $\partial/\partial\tau\rightarrow-U_{p+}\partial/\partial\mathcal{Z}$, respectively. By imposing these transformations, Eq. (18) appears in the following form:

$$(L_8-U_{p+})\frac{d\Phi}{d\mathcal{Z}}+L_1\Phi\frac{d\Phi}{d\mathcal{Z}}+L_2\frac{d^3\Phi}{d\mathcal{Z}^3}=0, \tag{19}$$

where U_{p+} is the phase speed of the drift IA wave, propagating in the direction of B_0. Equation (19) is the modified Korteweg–de Vries (mKdV) equation: it describes excitation of oblique drift IA solitary potentials. Thus by solving Eq. (19), the soliton solution is obtained, as

$$\Phi=\Phi_0\mathrm{sech}^2\left(\frac{\mathcal{Z}}{\Delta}\right). \tag{20}$$

The wave solution (20) is derived by imposing the boundary conditions $\Phi\rightarrow0$, $\partial\Phi/\partial\mathcal{Z}\rightarrow0$, and $\partial^2\Phi/\partial\mathcal{Z}^2\rightarrow0$ at $\mathcal{Z}\rightarrow\pm\infty$ on Eq. (19). The former represents a pulse-shaped drift IA soliton with amplitude $\Phi_0\{=3(U_{p+}-L_8)/L_1\}$ and spatial extension $\Delta\{=\sqrt{4L_2/(U_{p+}-L_8)}\}$, propagating in the inhomogeneous partially degenerate EI magnetoplasma. It is worth mentioning that the linear modes steepen upon self-interactions [39], and therefore ensue the drift IA solitary excitations, described by solution (20). The wave solution relies on the shallow water wave theory, where the long-wavelength water waves [40] encompass excitation of a nonlinear pulse whose amplitude is much smaller than the depth of water. Thus the solitary pulse, vanishing at $\mathcal{Z}\rightarrow\pm\infty$, also retains its shape during propagation. Importantly, solution (20) is valid for long timescale wave phenomena in which nonlinear steepening counterbalances the dispersion effect. Obviously, solution (20) attains real values for the spatial width (i.e., $\Delta^2>0$), as the phase speed exceeds the dimensionless dispersion, holding the $U_{p+}>L_8$ condition: it leads to excitation of the soliton. The spatial width of IA excitations, propagating with speed U_{p-} (opposite to B_0), turns out to be imaginary (i.e., $\Delta^2<0$) and therefore does not ensue a solitary pulse.

IV. INSTABILITY AND GROWTH RATE

The superimposition of drift IA waves by plane perturbations may cause instability, as the instability analysis of the mZK solitons have not been examined in the earlier studies [34–36]. Thus, for the instability analysis of the mZK equation (18), the small-k expansion scheme is modified. For this purpose, the stationary solution (20) is superimposed by plane perturbations [35,37] in the following form:

$$\Psi=\Phi(\mathcal{Z})+\psi(\mathcal{Z})\exp(i\mathrm{k}\mathcal{X}). \tag{21}$$

Here $\psi(\mathcal{Z})$ and $\Omega(\mathrm{k})$ represent amplitude function and angular frequency (wave number), respectively, of the perturbation, $\mathcal{X}(=l_\zeta\zeta+l_\eta\mathcal{Z}-\Omega\tau)$ is the phase angle, and $l_\zeta(l_\eta)$ designates the direction cosine parallel (perpendicular) to B_0. The frequency of perturbation is much smaller than the wave frequency, holding the $\Omega\ll\omega$ condition. Thus the amplitude function of the perturbation in Eq. (21) can be expressed in the form as

$$\psi(\mathcal{Z})=\psi_0(\mathcal{Z})+\mathrm{k}\psi_1(\mathcal{Z})+\mathrm{k}^2\psi_2(\mathcal{Z})\cdots. \tag{22}$$

The frequency of perturbation can be expanded as $\Omega=0+\mathrm{k}\Omega_1+\mathrm{k}^2\Omega_2\cdots$, where Ω_1 and Ω_2 are the next orders of Ω. Equation (22) is substituted into Eq. (18), and after setting $\Phi\rightarrow\Psi$, one obtains an expression for the zeroth-order amplitude function as

$$(-U_{p+}+L_1\Phi+L_8)\frac{\partial\psi_0}{\partial\mathcal{Z}}+L_2\frac{\partial^2\psi_0}{\partial\mathcal{Z}^2}=C, \tag{23}$$

where C is the constant of integration. Comparing Eqs. (23) and (19), after substituting $C = 0$ one arrives at the first solution as $\psi_0 = d\Phi/d\mathcal{Z} \equiv \mathcal{F}$. It has been checked that a second solution for Eq. (23) is $\psi_0 = \mathcal{F}\int \mathcal{F}^{-2} d\mathcal{Z} \equiv \mathcal{G}$. Thus the general solution for Eq. (23) can be given as

$$\psi_0 = C_1\mathcal{F} + C_2\mathcal{G} - C\mathcal{F}\int^{\mathcal{Z}} \frac{\mathcal{G}}{\mathcal{W}} d\mathcal{Z} + C\mathcal{G}\int^{\mathcal{Z}} \frac{\mathcal{F}}{\mathcal{W}} d\mathcal{Z}, \tag{24}$$

where C_1 and C_2 are arbitrary constants and $\mathcal{W}(= \mathcal{F}d\mathcal{G}/d\mathcal{Z} - \mathcal{G}d\mathcal{F}/d\mathcal{Z})$ corresponds to the Wronskian function. The solution for Eq. (23), converging at $\mathcal{Z} \to \pm\infty$, is given by

$$\psi_0 = C_1\mathcal{F}. \tag{25}$$

The perturbation scheme in Eqs. (18) and (22) is expanded beyond zeroth order [i.e., $\mathcal{O}$(k)] to obtain

$$\frac{d^2\psi_1}{d\mathcal{Z}^2} + \frac{(-U_{p+} + L_1\Phi + L_8)}{L_2}\psi_1 - \frac{iC_1}{L_2}\left\{a + b\tanh^2\left(\frac{\mathcal{Z}}{\Delta}\right)\right\}\Phi = C_3, \tag{26}$$

where C_3 is a constant of integration. The coefficients a and b, appearing in Eq. (26), are expressed in Appendix B. Solving Eq. (26), one obtains the following solution:

$$\psi_1 = C_4\mathcal{F} + \frac{iC_1\Delta^2}{8L_2}\left\{(a+b)\mathcal{F}\mathcal{Z} + \frac{2}{3}(3a+b)\Phi\right\}. \tag{27}$$

The constant of integration C_4 in Eq. (27) arises due to the characteristic solution. Notice that Eq. (27) vanishes (i.e., $\psi_1 \to 0$) at $\mathcal{Z} \to \pm\infty$ and corresponds to a nontrivial solution. At second-order approximation of the perturbation series $\mathcal{O}(\mathrm{k}^2)$, Eq. (18), leads to the following expression:

$$\left(-U_{p+}\frac{d}{d\mathcal{Z}} + L_1\frac{d\Phi}{d\mathcal{Z}} + L_2\frac{d^3}{d\mathcal{Z}^3} + L_8\frac{d}{d\mathcal{Z}}\right)\psi_2 = i\Omega_2\psi_0 + M_3\frac{\partial\psi_0}{\partial\mathcal{Z}} + i(\Omega_1 + U_{p+}l_\eta - L_7 l_\zeta - L_8 l_\eta + M_1)\psi_1 - iM_2\frac{d^2\psi_1}{d\mathcal{Z}^2}. \tag{28}$$

The coefficients M_1, M_2, and M_3 in Eq. (28) are given in Appendix B. Note that the first-order frequency (Ω_1) of perturbations determines the growth rate of instability. For the frequency Ω_1, one expresses the orthogonality condition of the solution (Φ) and the kernel (ψ_2) as

$$\int_{-\infty}^{\infty}\Phi\left\{i\Omega_2\psi_0 + M_3\frac{\partial\psi_0}{\partial\mathcal{Z}} + i(\Omega_1 + U_{p+}l_\eta - L_7 l_\zeta - L_8 l_\eta + M_1)\psi_1 - iM_2\frac{d^2\psi_1}{d\mathcal{Z}^2}\right\}d\mathcal{Z} = 0. \tag{29}$$

Equations (25)–(29), after some algebraic manipulation, lead to the perturbed frequency, as

$$\Omega_1 = \mathrm{Re}\ \Omega_1 + i(\mathrm{Im}\ \Omega_1), \tag{30}$$

where

$$\Omega_{1r} \equiv \mathrm{Re}\ \Omega_1 = \Lambda - l_\eta(U_{p+} - L_8) + l_\zeta L_7,$$
$$\text{and}\ \ \Omega_{1i} \equiv \mathrm{Im}\ \Omega_1 = (\Upsilon - \Lambda^2)^{1/2}. \tag{31}$$

Here $\Omega_{1r}(\Omega_{1i})$ is the real (imaginary) part of Ω_1. The algebraic form for Λ and Υ are given in Appendix B. It can be noticed that the perturbed frequency (Ω_1) significantly alters with variations in the dispersion coefficients of the mZK equation (16). Setting $L_7 = 0$ and $L_8 = 0$, the perturbed frequency in Eq. (30) reduces into the corresponding result of Refs. [34–36], obtained for the ZK equation. See from Eq. (31) that $\Omega_{1i} > 0$ when $\Upsilon > \Lambda^2$, revealing instability of the mZK soliton. By substituting Λ and Υ from Eqs. (44) and (45), respectively, into Eq. (31), one obtains the growth rate for the modified drift IA solitons, as

$$\gamma = \frac{\gamma_{\max}S^{\frac{1}{2}}}{\mathcal{N}_0^{\frac{1}{2}}\left(1 + \frac{\mathcal{N}_0\sin^2\theta}{\omega_r{}^2} - \frac{\mathcal{N}_0^{\frac{1}{2}}\mathrm{v_D}\sin\theta\cos\theta}{2\beta^{\frac{1}{2}}}\right)}, \tag{32}$$

where $\gamma_{\max}\{= 2l_\zeta(U_{p+} - L_8)\sqrt{(\mathcal{N}_0^2 + \omega_r{}^2)/15\omega_r{}^2}\}$ is the maximum value of γ. It can be readily checked from Eq. (32) that $\gamma \to \gamma_{\max}/\mathcal{N}_0^{\frac{1}{2}}$ when $\theta \to 0$. Importantly, $\gamma_{\max}^{-1}$ is the minimum time required for propagation of the unstable drift IA soliton. Here $S(= S_1 + S_2 + S_3)$ is the instability parameter, where S_1, S_2, and S_3 are given in APPENDIX B. Equation (32) is a novel expression illustrating the growth rate of the mZK solitons (20) that has not been elaborated in earlier studies [34–36]. More importantly, γ in Eq. (32) accounts for instability growth of the solitary potentials, impacted by two-dimensional perturbations and therefore alters with variations in obliqueness (θ). Moreover, the growth rate of the (p,2p)-mZk equation in Ref. [33] evaluates instability of the soliton, superimposed by one-dimensional perturbations: it is insensitive to variations in θ. It is important to mention that the growth rate in Eq. (32) can be used to obtain the characteristic length $d(\approx U_{p+}/\gamma)$ [41] for the unstable drift IA solitons. The instability criterion of the long-wavelength nonlinear excitations is also important in understanding anomalous diffusion in fusion plasmas. Combining Eqs. (22), (25), (27), and (30), one arrives at

$$\Psi = \mathrm{Re}\ \Psi + i(\mathrm{Im}\ \Psi). \tag{33}$$

The solution (33) represents drift IA soliton, superimposed by two-dimensional plane perturbations. The real and imaginary components of Ψ(i.e., Re Ψ and Im Ψ, respectively) are already given in Appendix B. Note that the small-k expansion scheme is applicable when the wave number of the perturbation is much smaller, holding the $\mathrm{k} \ll k$ condition. It has been checked from Eq. (32) that the angle (θ) of perturbing potential with the propagation vector ought to be <90°; otherwise $\gamma \to \infty$ and corresponds to an unphysical result.

V. NUMERICAL RESULTS AND DISCUSSION

For numerical illustration, some typical parameters of an inhomogeneous magnetoplasma have been taken, comprised of partially degenerate electrons and dynamical ions. The number density of plasma is $N_0 \sim 10^{27}$ cm^{-3}, the magnetic

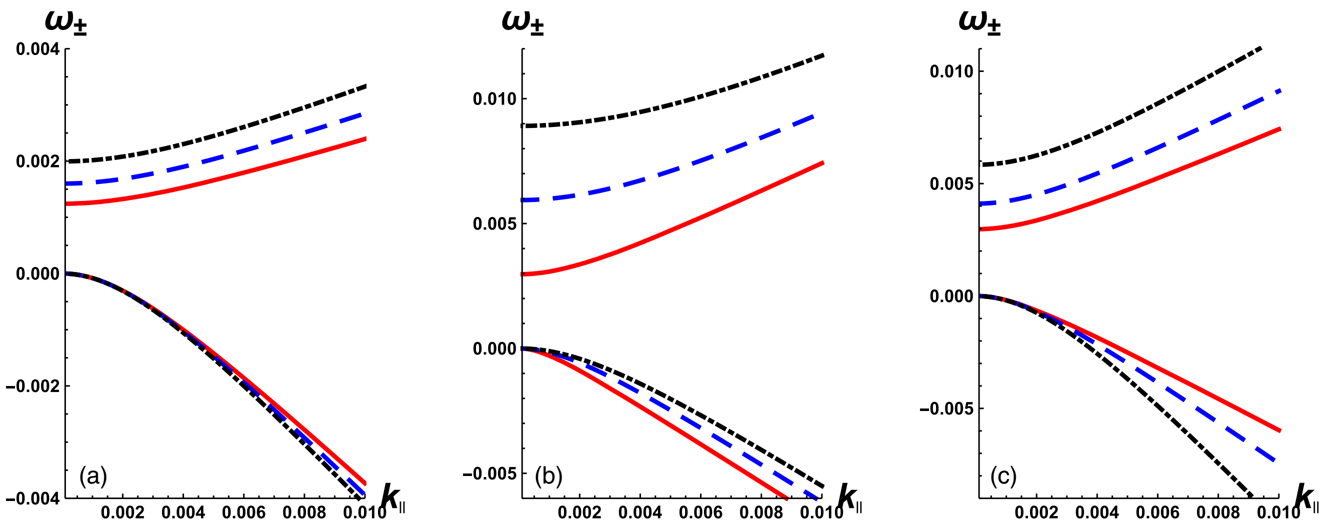

FIG. 1. (a) The angular frequencies from Eq. (11) are given at $B_0 = 10^{11}$ G (solid curve), 2×10^{11} G (dashed curve), and 3×10^{11} G (dotted curve). The frequencies are plotted in (b) at drift speed: $v_D = 0.1$ (solid curve), 0.2 (dashed curve), and 0.3 (dotted curve) and in (c) when the temperature ratio is $\Theta = 0.2$ (solid curve), 0.3 (dashed curve), and 0.4 (dotted curve).

field $B_0 \sim 10^{12}$ G, while the electron temperature is chosen to be $\mathcal{T}_e \sim 1$ keV. Such plasma has relevance to compact stars [5,6] and to high energy density facilities [42,43]. The ion drift, the temperature ratio, and the degeneracy parameter were computed as $v_D \sim 0.3$, $\Theta \sim 0.2$, and $X_{Fe} \sim 5$, respectively. Note that the growth rate is $\gamma \sim 0.002$ when the instability parameter attains positive values (i.e., $S > 0$). Thus the instability affects propagation of the drift IA solitons, as described in the following discussion.

The angular frequencies ($\omega_\pm$) of drift IA waves from Eq. (11) are plotted in Fig. 1(a) as a function of $k_\parallel$ at $B_0 = 10^{11}$ G (solid curve), 2×10^{11} G (dashed curve), and 3×10^{11} G (dotted curve). The upper (lower) branches represent the frequency of the drift IA wave, propagating in the direction of (opposite to) B_0. It reveals that intensification of B_0 enhances (reduces) $\omega_+(\omega_-)$ by impacting the ion gyration. As the frequency of the upper (lower) branches is $\omega_+ \approx \omega_*(\omega_- \approx 0)$ when $k_\parallel \approx 0$, it therefore constitutes an accelerated (decelerated) drift IA mode. To examine the impact of ion drift on the wave frequencies, Fig. 1(b) displays $\omega_\pm$ against $k_\parallel$ at $v_D = 0.1$ (solid curve), 0.2 (dashed curve), and 0.3 (dotted curve). Recall the ion drift enhances the frequency $\omega_*(= v_D k_\perp)$ and in turn rises $\omega_\pm$. Figure 1(c) depicts $\omega_\pm$ against $k_\parallel$ with variations in the temperature ratio, as $\Theta = 0.2$ (solid curve), 0.3 (dashed curve), and 0.4 (dotted curve). A degree enhancement in Θ increases (decreases) $\omega_+(\omega_-)$. The phase speed of the accelerated drift IA wave (U_{p+}) is illustrated versus $k_\parallel$ in Fig. 2(a) at different values of the magnetic field, as $B_0 = 10^{11}G$ (solid curve), $2 \times 10^{11}G$ (dashed curve), and 3×10^{11} (dotted curve). The

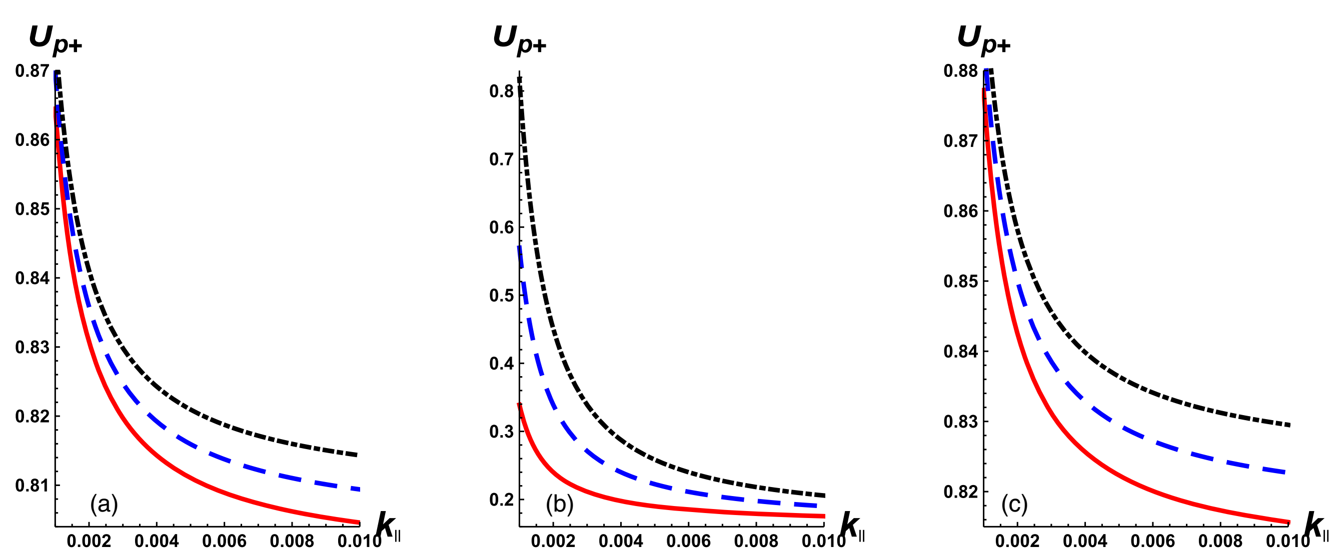

FIG. 2. (a) The phase speed [Eq. (12)] is given at $B_0 = 10^{11}$ G (solid curve), 2×10^{11} G (dashed curve), and 3×10^{11} G (dotted curve). The phase speed is also plotted in (b) at drift speed $v_D = 0.1$ (solid curve), 0.2 (dashed curve), and 0.3 (dotted curve) and in (c) at temperature ratio $\Theta = 0.2$ (solid curve), 0.3 (dashed curve), and 0.4 (dotted curve).

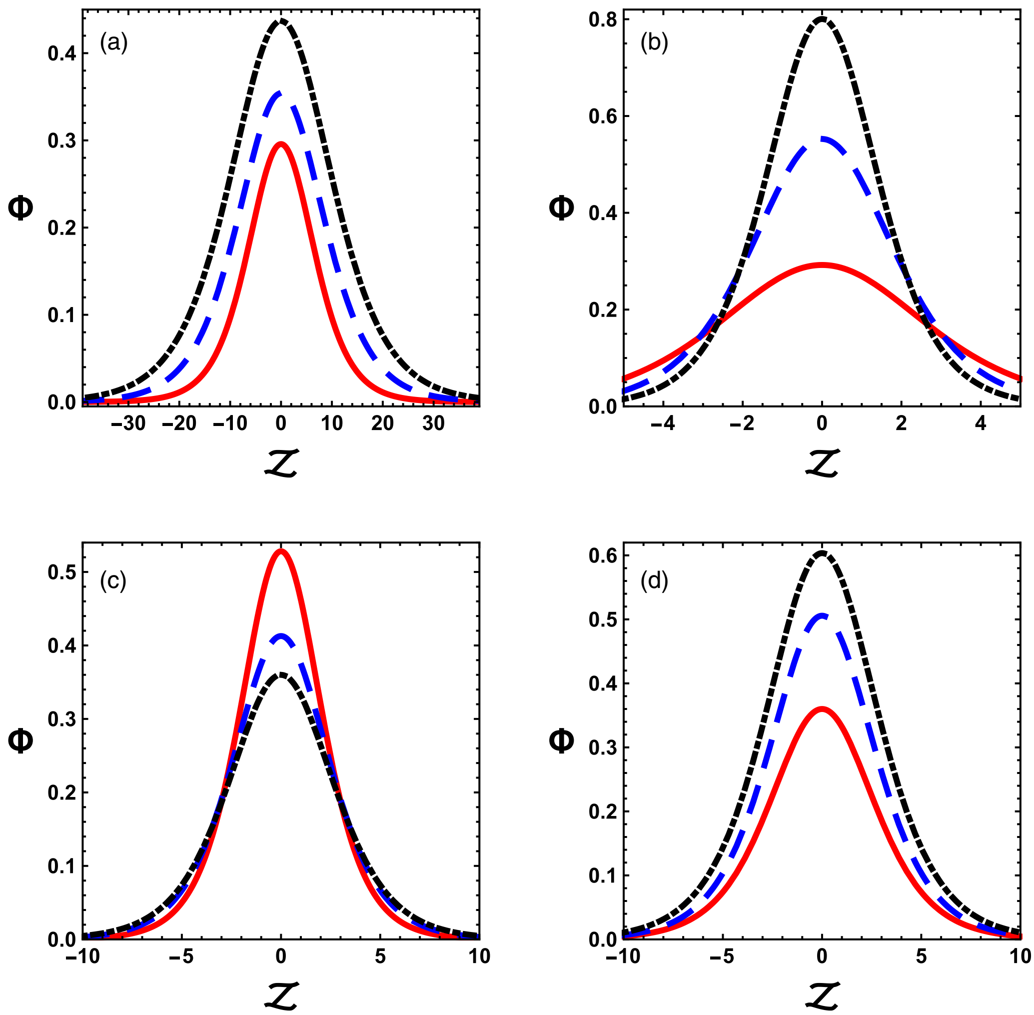

FIG. 3. The profile for drift IA soliton (20) is given vs $\mathcal{Z}$ at (a) obliqueness $\theta = 10^\circ$ (solid curve), 15° (dashed curve), and 20° (dotted curve), and (b) drift speeds $v_D = 0.1$ (solid curve), 0.3 (dashed curve), and 0.6 (dotted curve). The same are illustrated with variations in (c) temperature ratio $\Theta = 0.2$ (solid curve), 0.4 (dashed curve), and 0.6 (dotted curve) and (d) degeneracy parameter $X_{\mathrm{Fe}} = 2$ (solid curve), 3 (dashed curve), and 4 (dotted curve).

strength of B_0 enhances U_{p+} by increasing ω_+. Similarly U_{p+} is plotted as function of $k_\parallel$ in Fig. 2(b) (Fig. 2(c)) with variations in $v_D(\Theta)$. It can be noticed that an increase in the ion drift (electron temperature) leads to excitation of faster drift IA waves with relatively large U_{p+}. Note that the decelerated IA wave, attaining negative phase speed ($U_{p-} < 0$), and therefore cannot evolve solitary excitations, as highlighted in the forthcoming discussion.

The solitary wave solution (20) is displayed against the spatial variable ($\mathcal{Z}$) in Fig. 3(a) at $\theta = 10^\circ$ (solid curve), 15° (dashed curve), and 20° (dotted curve). It has been checked that the obliquity parameter tapers off (rises) the steepening (dispersion) coefficient, namely, $L_1(L_2)$, and therefore excites taller drift IA solitons with relatively wide spatial extension. Note that the spatial width $\Delta(=\sqrt{4L_2/U_{p-} - L_8})$ of decelerated drift IA mode is imaginary, as $U_{p-} < 0$ and $L_8 > 0$ conditions hold. Thus decelerated IA harmonics cannot evolve the solitary potential. The wave solution (20)—given in Fig. 3(b) at $v_D = 0.1$ (solid curve), 0.3 (dashed curve), and 0.6 (dotted curve)—shows that ion drift results in amplification (constriction) of the pulse amplitude (spatial extension). The profiles of solitary potential are illustrated in Fig. 3(c) at $\Theta = 0.2$ (solid curve), 0.4 (dashed curve), and 0.6 (dotted curve) and in Fig. 3(d) when $X_{\mathrm{Fe}} = 2$ (solid curve), 3 (dashed curve), and 4 (dotted curve). Thus parameter $\Theta(X_{\mathrm{Fe}})$, associating the thermal (trapping) effect to the electron, modifies the amplitude and spatial width of the wave. The parameter S in Eq. (32), designating the stability ($S < 0$) and the instability ($S > 0$) of drift IA excitations, has been displayed against θ at $B_0 = 10^{12}$G (solid curve), 1.2×10^{12}G (dashed curve), and 1.4×10^{12}G (dotted curve); refer to Fig. 4(a). The magnetic field strength leads to excitation of the unstable solitary waves by increasing the parametric region $S > 0$. Figure 4(b) depicts S versus θ at $v_D = 0.1$ (solid curve), 0.3 (dashed curve), and 0.6 (dotted curve). It can be seen that ion drift grows the instability, arising in the limit of $S > 0$. For the impact of electron temperature on instability, S has been given against θ in Fig. 4(c) at $\Theta = 0.2$ (solid curve), 0.4 (dashed curve), and 0.6 (dotted curve). Obviously, an increase in Θ gives rise to instability of the drift IA solitons. Contrary to this, the instability parameter depicted at different values of X_{Fe} in Fig. 4(d) shifts S to negative values. Thus the trapped

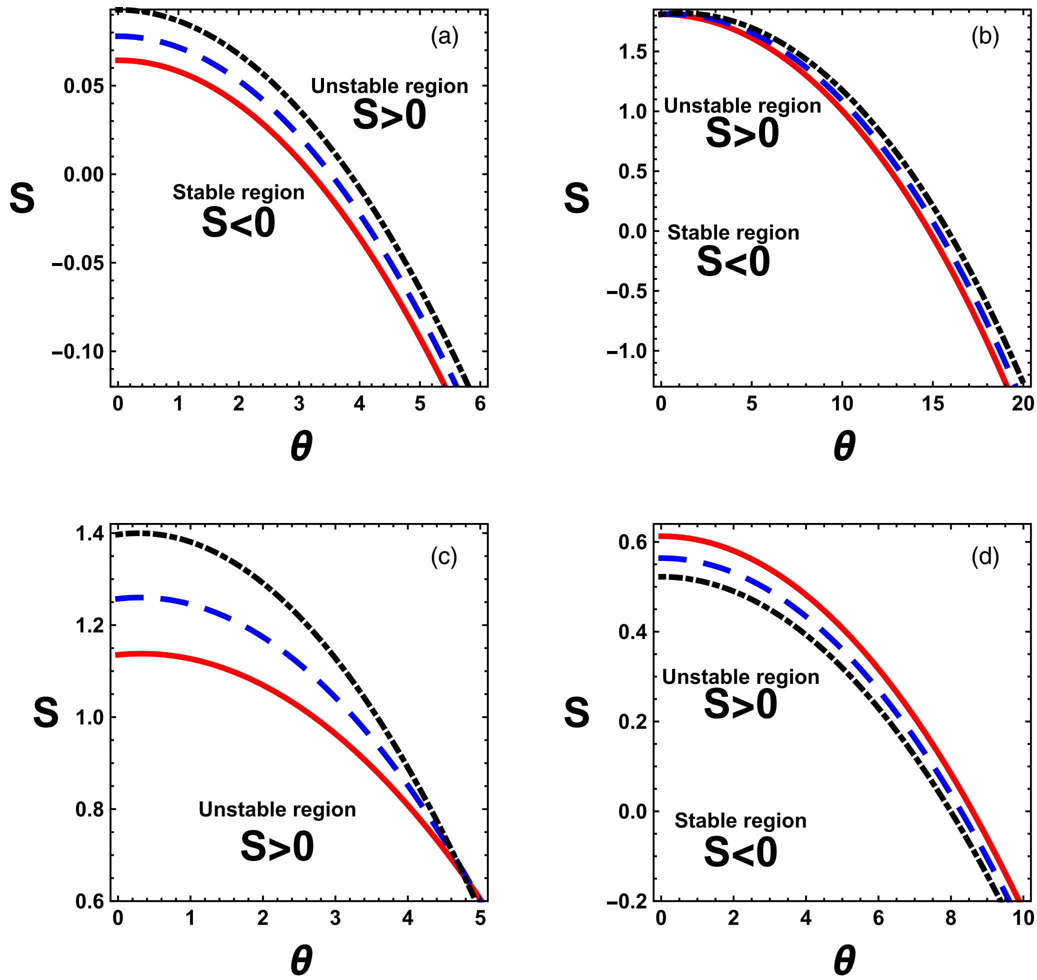

FIG. 4. The instability parameter (S) is given against θ at (a) $B_0 = 10^{12}$ G (solid curve), 1.2×10^{12} G (dashed curve), and 1.4×10^{12} G (dotted curve) and (b) $v_D = 0.1$ (solid curve), 0.3 (dashed curve), and 0.6 (dotted curve). The parameter S is depicted at different values of (c) temperature ratio $\Theta = 0.2$ (solid curve), 0.4 (dashed curve), and 0.6 (dotted curve) and (d) degeneracy parameter $X_{Fe} = 2$ (solid curve), 3 (dashed curve), and 4 (dotted curve).

electrons evolve the drift IA solitons that are stable against the perturbations.

By using Eq. (32), the growth rate is plotted against θ in Fig. 5(a) with variation in the magnetic field as $B_0 = 10^{12}$G (solid curve), 1.2×10^{12}G (dashed curve), and 1.4×10^{12}G (dotted curve). This infers that at $\theta \leqslant (>)2$, the magnetic field causes γ to decrease (increase) by reducing (enhancing) the wave instability. Figure 5(b) illustrates γ versus θ at $v_D = 0.1$ (solid curve), 0.3 (dashed curve), and 0.6 (dotted curve). The ion drift amplifies the pulse amplitude and in turn increases γ. Similarly, γ is plotted against θ in Figs. 5(c) and Fig. 5(d), changing the temperature ratio and the degeneracy parameter, respectively. The electron temperature causes the wave dispersion, thus enhancing the growth rate of instability. The trapped electrons, on the other hand, steepen the wave, giving rise to γ. Note that the growth rate of instability shortens the propagation span (τ) of a wave, as $\tau = \gamma^{-1}$. Thus the drift IA waves that excite at small (large) angle of the magnetic field achieve a relatively large (vanishingly small) growth rate and therefore survive for a short (long) period.

The imaginary part of the perturbation-superimposed wave solution in Eq. (33) is given versus $\mathcal{Z}$ in Fig. 6(a) at $\theta = 1^\circ$ (solid curve), 4° (dashed curve), and 8° (dotted curve) when the growth rate is $\gamma = 0.002,\ 0.001$, and 0.0006, respectively. It can be noticed that the obliqueness of a solitary pulse along with the perturbations reduces γ, which stabilizes the wave. The imaginary solution (Im Ψ), given in Fig. 6(b) at various values of v_D, infers that ion drift enhances γ and therefore leads to temporal growth of the wave. Similarly, by varying B_0 and X_{Fe}, Im Ψ has been given against $\mathcal{Z}$ in Figs. 6(c) and 6(d), respectively. The magnetic field (degeneracy parameter) causes decay (growth) of the wave as it suppresses (grows) the instability, see Figs. 5(a) and 5(b). By solving Eq. (32), the frequency ratio (ω_r) is given versus θ and v_D, respectively, in Figs. 7(a) and 7(b) . Note that the solid curves therein correspond to a *critical frequency* (ω_{rc}), where the instability parameter and the growth rate vanish ($S = \gamma = 0$). Moreover, the lower (upper) shadings represent stable (unstable) drift IA solitary potentials with frequency less than or equal to (greater than) ω_r. The enhancement in obliquity parameter (ion drift) extends the frequency domain $\omega_r \leqslant \omega_{rc}$ ($\omega_r > \omega_{rc}$), evolving the stable (unstable) excitations. The frequency ratio, plotted versus Θ and X_{Fe} in Figs. 7(c) and 7(d), respectively, indicates that electron temperature (degeneracy) widens the frequency

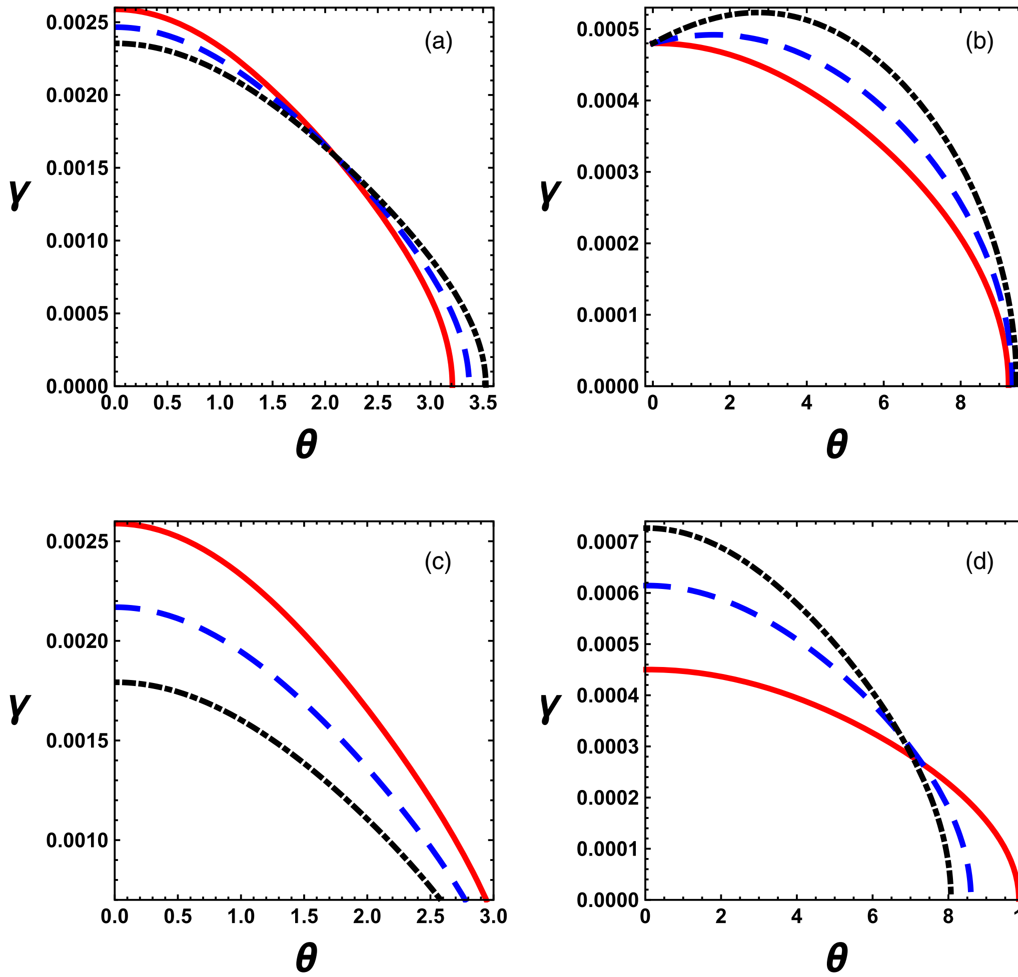

FIG. 5. The growth rate (γ) from Eq. (32) is given vs θ in (a) at $B_0 = 10^{12}$ G (solid curve), 1.2×10^{12} G (dashed curve), and 1.4×10^{12} G (dotted curve) and in (b) when $v_D = 0.1$ (solid curve), 0.3 (dashed curve), and 0.6 (dotted curve). The growth rate is also illustrated at different values of (c) temperature ratio $\Theta = 0.2$ (solid curve), 0.4 (dashed curve), and 0.6 (dotted curve) and (d) degeneracy parameter $X_{\mathrm{Fe}} = 2$ (solid curve), 3 (dashed curve), and 4 (dotted curve).

regime for unstable (stable) IA solitons. It has been pointed out [44] that the instability gives rise to anomalous diffusion (D) that varies proportionally with growth rate (i.e., $D \propto \gamma$). Since the drift IA waves in the frequency regime $\omega_r \leqslant \omega_{rc}$ have attained zero growth rate, they are not affected by the diffusion.

VI. SUMMARY

The propagation characteristics and stability (instability) of modified solitons have been examined in an inhomogeneous magnetoplasma, containing partially degenerate electrons and dynamical ions. Astrophysical objects, including white dwarfs, magnetars, neutron stars, etc., as well as high energy density facilities, are possible outlets for the plasma. For the purpose, a modified Zakharov-Kuznetsov equation (16) is derived that admits a pulse-shaped solitary wave in the limit when phase velocity exceeds the dispersion effect. A modification of the small-k expansion method leads to the growth rate (32) of the mZK soliton, which has not been described elsewhere. Furthermore, the obtained result reduces into the growth rate of ZK solitons [34–36] in an appropriate limit. The ion drift energizes solitary waves, increasing their amplitude and hence instabilities. Similarly, the degeneracy parameter (X_{Fe}) alters concentration of the trapped electrons and in turn modifies γ. The solitary pulses achieve relatively low growth rates while propagating at large obliqueness and therefore last for a long time. More importantly, the drift IA waves whose frequency is less than or equal to the critical frequency ($\omega_r \leqslant \omega_{rc}$) do not cause the anomalous diffusion, as these are stable to perturbations. This study is important to understand the instability of the modified drift IA waves that may cause deconfinement of matter in the fusion scheme.

The data that support findings of this study, are available within the article.

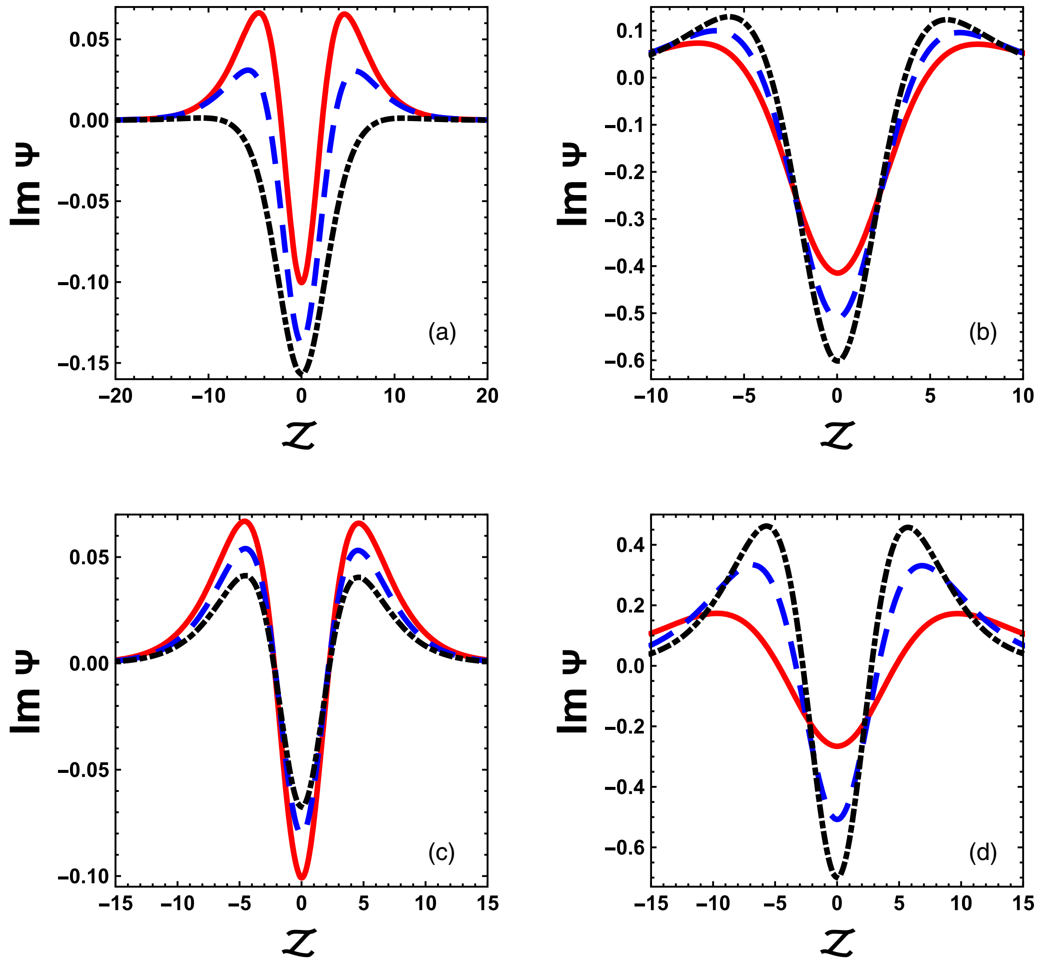

FIG. 6. The imaginary part of solution (33) is displayed vs $\mathcal{Z}$ at (a) $\theta = 1^\circ$ (solid curve), 4° (dashed curve), and 8° (dotted curve) and (b) $\mathrm{v_D} = 0.1$ (solid curve), 0.3 (dashed curve), and 0.6 (dotted curve). The solution Im Ψ is depicted at (c) magnetic field $B_0 = 10^{12}$ G (solid curve), 1.2×10^{12} G (dashed curve), 1.4×10^{12} G (dotted curve), and 0.6 (dotted curve) and (d) degeneracy parameter $X_{\mathrm{Fe}} = 2$ (solid curve), 3 (dashed curve), and 4 (dotted curve).

APPENDIX A: COEFFICIENTS OF EQ. (18)

The coefficients, appearing in Eq. (18), are given by

$$L_1 = \cos\theta, \quad L_2 = \mathrm{B}\cos\theta\sin^2\theta + \mathrm{C}\cos^3\theta + \mathrm{E}\sin\theta\cos^2\theta, \tag{A1}$$

$$L_3 = -\sin\theta, \quad L_4 = -\mathrm{B}\sin\theta\cos^2\theta - \mathrm{C}\sin^3\theta + \mathrm{E}\sin^2\theta\cos\theta, \tag{A2}$$

$$L_5 = \mathrm{B}(2\cos^2\theta - \sin^2\theta)\sin\theta - 3\mathrm{C}\sin\theta\cos^2\theta + \mathrm{E}(\cos^2\theta - 2\sin^2\theta)\cos\theta, \tag{A3}$$

$$L_6 = \mathrm{B}(\cos^2\theta - 2\sin^2\theta)\cos\theta + 3\mathrm{C}\sin^2\theta\cos\theta + \mathrm{E}(\sin^2\theta - 2\cos^2\theta)\sin\theta, \tag{A4}$$

and

$$L_7 = -\mathrm{A}\sin\theta + \mathrm{D}\cos\theta, \quad \text{and} \quad L_8 = \mathrm{A}\cos\theta + \mathrm{D}\sin\theta. \tag{A5}$$

APPENDIX B: COEFFICIENTS OF EQS. (26)–(33)

The coefficients in Eqs. (26) and (27) are given by

$$a = \Omega_1 + l_\eta(U_p - L_8) - l_\zeta L_7 - \frac{\Phi_0 M_1}{2} + \frac{2M_2}{\Delta^2}, \quad \text{and} \quad b = \frac{\Phi_0 M_1}{2} - \frac{6M_2}{\Delta^2}, \tag{B1}$$

with

$$M_1 = L_1 l_\eta + L_3 l_\zeta, \quad \text{and} \quad M_2 = 3L_2 l_\eta + L_5 l_\zeta. \tag{B2}$$

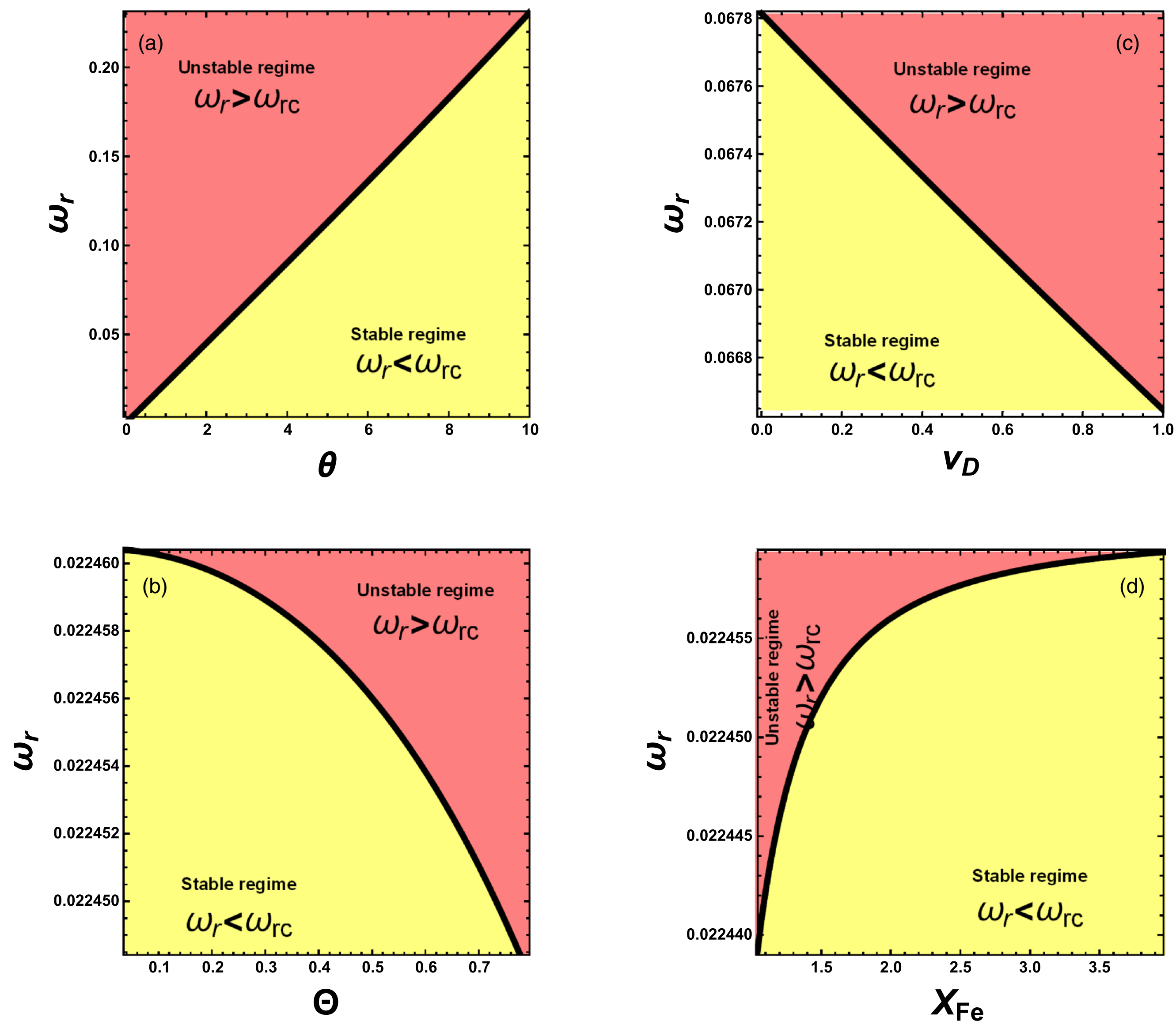

FIG. 7. The frequency ratio (ω_r) is depicted vs (a) obliqueness θ and (b) drift speed $\mathrm{v_D}$. The frequency ratio is given against (c) temperature ratio Θ and (d) degeneracy parameter X_{Fe}.

The expansion coefficient, arising at the second-order approximation [in Eqs. (28) and (29)] can be expressed as

$$M_3 = 3L_2 {l_\eta}^2 + L_6 {l_\zeta}^2 + L_5 l_\eta l_\zeta. \tag{B3}$$

Note that the coefficient M_3 in Eq. (B3) matches exactly to the earlier result [34,35] when $l_\eta = 0$ therein [34,35]. The perturbed frequencies in the dispersion relation (31) are given as

$$\Lambda = \frac{2}{3}\left(M_1\Phi_0 - 2\frac{M_2}{\Delta^2}\right), \tag{B4}$$

and

$$\Upsilon = \frac{16}{45}\left({M_1}^2{\Phi_0}^2 - 3\frac{\Phi_0 M_1 M_2}{\Delta^2} - 3\frac{M_2^2}{\Delta^4} + 12\frac{M_3 L_2}{\Delta^4}\right). \tag{B5}$$

The parameters S_1, S_2, and S_3 [$S(= S_1 + S_2 + S_3)$ in Eq. (32)] are given by

$$S_1 = 1 - \frac{5\mathcal{N}_0 \tan^2\theta}{3} - \frac{5\mathcal{N}_0^2 \tan^2\theta}{3{\omega_r}^2}, \tag{B6}$$

$$S_2 = \frac{\mathcal{N}_0^{\frac{3}{2}} \mathrm{v_D} \sin^2\theta \tan\theta}{6(\mathcal{N}_0^2 + \omega_r{}^2)\beta^{\frac{1}{2}}} \left\{ 3(\omega_r{}^2 + \mathcal{N}_0 \sin^2\theta) + 2(\mathcal{N}_0 + \omega_r{}^2)\sin^2\theta - \frac{\mathcal{N}_0^{\frac{1}{2}} \mathrm{v_D} \omega_r{}^2}{\beta^{\frac{1}{2}} \sin^2\theta \tan\theta} \right\}, \tag{B7}$$

and

$$S_3 = \frac{\mathrm{v_D} \cos\theta \sin\theta (7\omega_r{}^2 + 5\mathcal{N}_0 - 2\omega_r{}^2\cos^2\theta + 5\mathcal{N}_0 \sin^2\theta)}{6(\mathcal{N}_0^2 + \omega_r{}^2)\beta^{\frac{1}{2}}}. \tag{B8}$$

The real and imaginary components of Ψ, marked as Re Ψ and Im Ψ in Eq. (33), can be algebraically expressed as

$$\begin{aligned} \mathrm{Re}\ \Psi = \Phi + \Bigg[&(\psi_0 + \mathrm{k} C_4 \mathcal{F}) \cos \mathrm{k}\mathcal{X}_r - \mathrm{k}\frac{C_1 \Delta^2}{8L_2} \left\{ (a_r + \beta)\mathcal{F}\mathcal{Z} + \frac{2}{3}(3a_r + b)\Phi \right\} \sin \mathrm{k}\mathcal{X}_r \\ &- \mathrm{k}\frac{C_1 \Delta^2}{8L_2}(a_i \mathcal{F}\mathcal{Z} + 2a_i \Phi)\cos \mathrm{k}\mathcal{X}_r \Bigg] \exp(\mathrm{k}\mathcal{X}_i), \end{aligned} \tag{B9}$$

and

$$\mathrm{Im}\ \Psi = \left[(\psi_0 + \mathrm{k} C_4 \mathcal{F}) \sin \mathrm{k}\mathcal{X}_i + \frac{C_1 \Delta^2}{8L_2} \left\{ (a_r + b)\mathcal{F}\mathcal{Z} + \frac{2}{3}(3a_r + b)\Phi \right\} \cos \mathrm{k}\mathcal{X}_i + \frac{C_1 \Delta^2 a_i}{8L_2}(\mathcal{F}\mathcal{Z} + 2\Phi)\sin \mathrm{k}\mathcal{X}_i \right] \exp(\mathrm{k}\mathcal{X}_r), \tag{B10}$$

where $\mathcal{X}_r (= l_\zeta \zeta + l_\eta \mathcal{Z} - \Omega_{1r}\tau)$ and $\mathcal{X}_i (= \Omega_{1i}\tau)$ are the real and imaginary parts of $\mathcal{X}$; moreover, $a_r = \Lambda - \frac{\Phi_0 M_1}{2} + \frac{2M_2}{\Delta^2}$ and $a_i = (\Upsilon - \Lambda^2)^{\frac{1}{2}}$.

[1] L. K. Ang, T. J. T. Kwan, and Y. Y. Lau, Phys. Rev. Lett. **91**, 208303 (2003).
[2] D. Liu, X. Chen, Y. Hu, T. Sun, Z. Song, Y. Zheng, Y. Cao, Z. Cai, M. Cao, L. Peng, Y. Huang, L. Du, W. Yang, G. Chen, D. Wei, A. Thye S. Wee, and D. Wei, Nat. Commun. **9**, 193 (2018).
[3] G. Manfredi and P.-A. Hervieux, Appl. Phys. Lett. **91**, 061108 (2007).
[4] A. Moradi, J. Phys.: Condens. Matter **21**, 045303 (2009).
[5] M. Opher, L. O. Silva, D. E. Dauger, V. K. Decyk, and J. M. Dawson, Phys. Plasmas **8**, 2454 (2001).
[6] Y. D. Jung, Phys. Plasmas **8**, 3842 (2001).
[7] M. Marklund and P. K. Shukla, Rev. Mod. Phys. **78**, 591 (2006).
[8] R. Thiele, P. Sperling, M. Chen *et al.*, Phys. Rev. E **82**, 056404 (2010).
[9] I. B. Bernstein, J. M. Greene, and M. D. Kruskal, Phys. Rev. **108**, 546 (1957).
[10] A. V. Gurevich, L. V. Pariskaya, and L. P. Pitaevskii, Zh. Eksp. Teor. Fiz. **49**, 647 (1965) [Sov. Phys. JETP **22**, 449 (1966)].
[11] J. Weiland, *Collective Modes in Inhomogeneous Plasma* (Institute of Physics, Bristol, 2000).
[12] B. B. Kadomtsev and O. P. Pogutse, Nucl. Fusion **11**, 67 (1971).
[13] F. F. Chen, *Introduction to Plasma Physics and Controlled Fusion* (Plenum, New York, 1983).
[14] V. L. Krasovsky, H. Matsumotoa, and Y. Omura, J. Geophys. Res. **102**, 22131 (1997).
[15] E. Oz, S. Deng, T. Katsouleas, P. Muggli, C. D. Barnes, I. Blumenfeld, F. J. Decker, P. Emma, M. J. Hogan, R. Ischebeck *et al.*, Phys. Rev. Lett. **98**, 084801 (2007).
[16] H. A. Shah, M. N. S. Qureshi, and N. Tsintsadze, Phys. Plasmas **17**, 032312 (2010).
[17] N. L. Tsintsadze, H. A. Shah, M. N. S. Qureshi, and M. N. Tagviashvili, Phys. Plasmas **22**, 022303 (2015).
[18] M. Irfan, S. Ali, and Arshad M. Mirza, Phys. Plasmas **24**, 052108 (2017).
[19] B. B. Jones and R. Wilson, Nucl. Fussion Suppl. **3**, 889 (1962).
[20] N. Vianello, M. Spolaore, E. Martines, R. Cavazzana, G. Serianni, M. Zuin, E. Spada, and V. Antoni, Nucl. Fusion **50**, 042002 (2010).
[21] M. Salimullah, M. Jamil, H. A. Shah, and G. Murtaza, Phys. Plasmas **16**, 014502 (2009).
[22] D. Montgomery, Phys. Fluids **3**, 274 (1960).
[23] G. Rowlands, J. Plasma Phys. **3**, 567 (1969).
[24] E. Infeld, J. Plasma Phys. **33**, 171 (1985).
[25] A. A. Mamun and R. A. Cairns, J. Plasma Phys. **56**, 175 (1996).
[26] F. Haas, *Quantum Plasma: An Hydrodynamic Approach* (Springer, New York, 2011).
[27] M. L. Kutner, *Astronomy: A Physical Perspective* (Cambridge University Press, New York, 2003).
[28] L. D. Landau and E. M. Lifshitz, *Statistical Physics* (Butterworth-Heinemann, Oxford, 1980).
[29] M. Irfan, S. Ali, and A. M. Mirza, Phys. Plasmas **26**, 032101 (2019).
[30] S. L. Shapiro and S. L. Teukolsky, *Black Holes, White Dwarf, and Neutron Stars* (Wiley, New York, 2004).
[31] R. Bowley and M. Sánchez, *Introductory Statistical Mechanics*, 2nd ed. (Clarendon Press, Oxford, 1999).
[32] A. Ahmad and W. Masood, J. Plasma Phys. **81**, 905810505 (2015).
[33] N. Hongsit, M. A. Allen, and G. Rowlands, Phys. Lett. A **372**, 2420 (2008).
[34] A. A. Mamun, Phys. Scr. **58**, 505 (1998).
[35] A. A. Mamun, S. M. Russella, C. A. M.- Bricennoa *et al.*, Planet. Space Sci. **48**, 163 (2000).
[36] E. E. Behery, F. Haas, and I. Kourakis, Phys. Rev. E **93**, 023206 (2016).
[37] S. K. El-Labany, W. F. El-Taibany, and E. E. Behery, Phys. Rev. E **88**, 023108 (2013).
[38] H. Washimi and T. Taniuti, Phys. Rev. Lett. **17**, 996 (1966).
[39] W. M. Moslem, R. Sabry, S. K. El-Labany, and P. K. Shukla, Phys. Rev. E **84**, 066402 (2011).

[40] L. Debnath, *Nonlinear Partial Differential Equations for Scientists and Engineers*, 2nd ed. (Birkhäuser, Boston, MA, 2004).
[41] B. B. Kadomtsev, *Plasma Turbulance* (Academic Press, London, 1965).
[42] S. J. Rose, Plasma Phys. Controlled Fusion **47**, B735 (2005).
[43] S. H. Glenzer and R. Redmer, Rev. Mod. Phys. **81**, 1625 (2009).
[44] J. W. Connor and O. P. Pogutse, Plasma Phys. Control. Fusion **43**, 155 (2001).